Copyright © 2002 Tech Science Press CMES, vol.3, no.3, pp.299-312, 2002

Computer Modeling and Simulation of Stationary-Vane, Rolling Piston Refrigeration Compressors

G. Prater, Jr.[1]

Abstract: A vapor compressor's performance is affected by pressure and mass flow fluctuations resulting from acoustic effects in the suction and discharge manifolds. Through proper geometric design of the manifolds, these pulsations can be modified to increase efficiency and reduce noise. This paper documents the development of a computer simulation program used to tune stationary-vane refrigeration compressors. The program models the mechanical, fluid, thermodynamic, kinematic, and acoustical processes occurring in such compressors, and calculates suction and discharge chamber pressures, mass flow rates, valve displacements, and acoustic input and transfer impedances. Experimental acoustic pressure measurements from a refrigerator test stand provide validation of the simulation results.

keyword: Compressor, rolling piston, refrigeration, fluid power, acoustic tuning, mathematical modeling.

1 Introduction

The development of rolling piston vapor compressors represents one response by the major appliance industry to the need for efficient, quiet, and low cost household refrigerators (Sartre, Lallemand, and Chiaffi, 1994). These machines are designed about a shaft-mounted eccentric rotating within a stationary cylinder (Fig. 1). An annular "rolling piston" on the eccentric reduces friction and wear due to relative motion between surfaces. Suction and compression working volumes exist simultaneously, separated by a spring-loaded stationary vane and an oil-film clearance between the eccentric and cylinder. As the eccentric rotates, the size of the suction volume increases, while that of the discharge volume decreases. Refrigerant state in the discharge line is critical to system performance, so the pressure in the compression volume is regulated through the use of a reed valve. Because the refrigerant state during the suction process is not critical, machines of this type often dispense with suction valves as a cost reduction measure. An AC electric motor drives the shaft. The entire assembly is contained within a hermetically sealed shell, through which pass the electrical power supply, a refrigerant suction line, and a refrigerant discharge line.

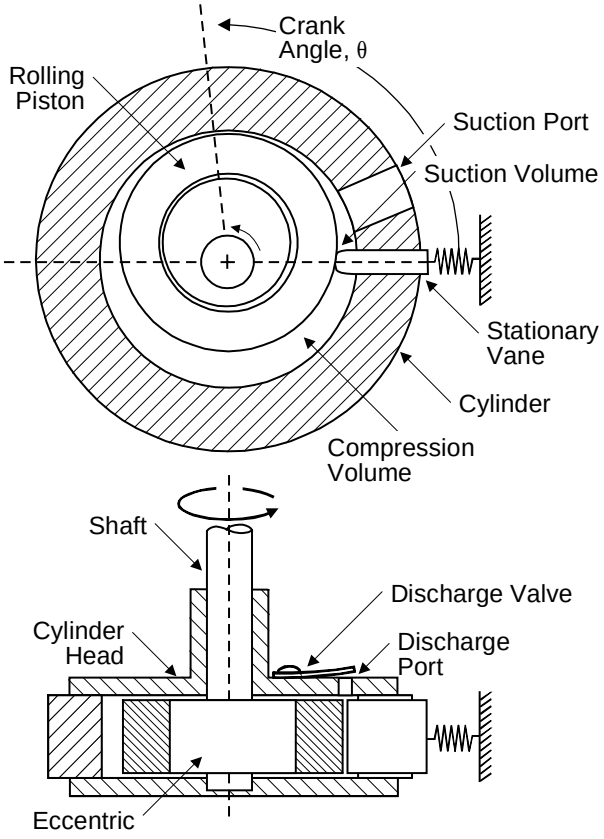

Figure 1 : Mechanical components of a rolling piston vapor compressor

The cyclic nature of the processes in vapor compressors means that there is always a potential for vibra-

[1] Department of Mechanical Engineering
University of Louisville
Louisville, KY 40292 USA

tion and acoustic transmission along structural and fluid paths. Structural vibration is a significant noise source, and results in a requirement for expensive mounting systems. Acoustic effects in the refrigerant vapor create pressure and flow rate fluctuations in the suction and discharge lines. These pulsations are most pronounced in the discharge system, where they are considered detrimental and eliminated, if possible, through the use of mufflers. Unfortunately, mufflers increase backpressure, which lowers volumetric efficiency and increases power consumption. Through proper geometric design of the manifolds and valves, flow pulsations can be modified to increase efficiency and reduce noise.

Suction and discharge processes in such machines are periodic and unsteady; thus, they give rise to mass flow and pressure fluctuations in the manifold systems. Such pulsations are a result of longitudinally propagating acoustic plane waves that affect both noise levels and efficiency by modifying the refrigerant flow rates. The magnitude and frequency of these waves are in turn influenced by the manifold geometries. It is possible to modify, or tune, manifold geometry to increase efficiency or reduce noise. Experimental tuning is very expensive, especially when performed early in the product development process. Consequently, a computer simulation program that models the acoustic phenomena and computes performance parameters would be a useful design tool.

As part of an acoustic tuning research project, we have developed such a simulation program. RSIMP (Rolling piston compressor Simulation Program) models the mechanical, thermodynamic, valve flow, kinematic, and acoustical processes occurring in rolling piston vapor compressors. A polytropic model is used for the compression and expansion processes. One set of subroutines determines acoustic input and transfer impedances of the suction and discharge manifolds. Other routines model the flow processes, valve dynamics, and kinematic behavior of the system. The program numerically solves the coupled governing equations for working volume pressures, mass flow rates, valve displacement, and manifold pressures. These primary time domain variables are then used to calculate various compressor performance parameters. Simulation results are written to a formatted output file and displayed graphically.

The first version of RSIMP used Fortran 90 as the development environment. However, the latest version was ported to Microsoft Visual Basic so that a Windows graphical user interface could be added.

2 Review of Previous Work

Existing literature on vapor compressors is quite extensive, but most computer simulation work has been limited to reciprocating machines (Soedel, 1972; Hamilton, 1974). Acoustic effects were incorporated into single cylinder and multiple cylinder models through work performed by Singh and Soedel (1979). Nieter (1983) developed a comprehensive simulation program using acoustic transfer matrices to model multiple cylinder reciprocating machines and conduct parametric tuning studies. The literature on rolling piston type vapor compressors is more limited, and there are few examples of simulation programs for these machines. Ooi and Wonga (1997) developed a program based upon a general purpose performance model that included mechanical losses and the compressor thermodynamic cycle; however, their simulation did not include acoustic effects. Park, Kim and Min (2001) used a very simple rolling piston compressor model as part of an analysis of a multi-type inverter air conditioner. Padhy and Dwivedi (1994) modeled the heat transfer processes in such machines for the purpose of improving energy efficiency.

Most rolling piston compressor research has addressed specific design issues. Examples include investigations of kinematics and kinetics (Okada and Kuyama, 1982; Yanagisawa and Shimizu, 1982), transient characteristics (Yanagisawa, Shimizu, and Horioka, 1988; Ishii, Imaichi, and Muramatsu, 1984), tribology (Okoma and Onoda, 1988; Hadfielda and Safarib, 1998), bearing performance (Itami, Kubo, and Sugiyama, 1986; Jorgensen and Nissen, 1984), vane configuration (Chai and Ooi, 1995), and valve design (Sa, Kim, Son, Park, and Byun, 1992; Ooi, Chai, and Kwek, 1992; Sheiretov, Van Glabbeek, and Cusano, 1995).

A number of investigators have worked to enhance the algorithms that can be applied to the numerical analysis of thermo-fluid processes inherent to studies of machines of this type. Lin and Atluri (2000) investigated a meshless local Petrov-Galerkin (MLPG) method applied to convection-diffusion problems. Lin and Atluri (2001) also used the same general approach to solve the incompressible Navier-Strokes equations. Rugonyi and Bathe (2001) used a finite element method to analyze fluid flow with coupled with structural interaction, which can be an issue with the suction and discharge manifolds on refrig-

eration compressors.

3 Theory

RSIMP embodies mathematical models for the cylinder kinematics and thermodynamics, valve dynamics, fluid flow through the valve, acoustic characteristics of the suction and discharge manifolds, and interaction between the cylinder and manifolds. Program assumptions include:

- Polytropic equation of state for the charging and compression processes
- Ideal gas working fluid
- One-dimensional fluid flow through the valves and manifold systems
- Constant drive motor angular velocity
- Suction chamber nominal fluid state is the same as that of the refrigerant at the suction port
- Damped, single degree-of-freedom valve displacement model
- Unsteady, compressible flow through the valve
- Acoustic plane wave theory is valid

Fluid leakage, cylinder heat transfer, lubrication effects, variable rolling piston velocity, friction, and motor dynamics are not directly modeled.

3.1 Kinematic Model

The kinematic model represents the steady state chamber volume as a function of the crank angle, θ:

$$V(\theta) = V_t - \frac{1}{2}R^2h\theta + \frac{1}{2}r^2h(\theta+\alpha) + \ldots + \frac{1}{2}eh(r+r_v)\sin(\theta+\alpha) - \frac{1}{2}r_v^2h\tan\alpha - \frac{1}{2}bhx, \quad (1a)$$

$$V_t = \pi(R^2 - r^2)h, \quad (1b)$$

$$\alpha = \sin^{-1}\left[\frac{e}{(r+r_v)}\sin\theta\right], \quad (1c)$$

$$x = R + r_v - (r+r_v)\cos\alpha - e\cos\theta. \quad (1d)$$

V_t	=	total volume
h	=	cylinder height
R	=	cylinder radius
r	=	roller radius
e	=	relative eccentricity, $R-r$
r_v	=	vane tip radius
b	=	vane thickness
x	=	vane extension past cylinder
α	=	calculation constant

The mean volumetric flow rate then becomes:

$$\frac{dV}{dt} = \frac{1}{2}\left[eh\omega + r^2h\frac{d\alpha}{dt} + eh(r+r_v)(\omega+\frac{d\alpha}{dt})\cos(\alpha+\theta) - \ldots - r_v^2h\sec^2\alpha\frac{d\alpha}{dt} - bh\frac{dx}{dt} - r_v^2h\sec^2\alpha\frac{d\alpha}{dt} - bh\frac{dx}{dt}\right], \quad (2a)$$

$$\frac{dx}{dt} = (r+r_v)\sin\alpha + e\omega\sin\theta, \quad (2b)$$

$$\frac{d\alpha}{dt} = \frac{e\omega_0\cos\theta}{r+r_v}\left[1 - \left(\frac{e}{r+r_v}\sin\theta\right)^2\right]^{-\frac{1}{2}}, \quad (2c)$$

$$\omega_0 = \frac{d\theta}{dt} = \text{constant}. \quad (2d)$$

The crank speed, ω_0, is equal to the motor angular velocity.

3.2 Thermodynamic Model

The working fluid in the simulation program is assumed to behave as an ideal gas, p_cv_c=R_gT_c, where p_c, v_c, and T_c are the chamber pressure, specific volume, and temperature, respectively, and R_g is the universal gas constant. When this expression is combined with a polytropic process model, $p_cv_c^n$ =constant, the state of the refrigerant in the compression chamber can be established using the following relations:

$$p_c(\theta) = \left(\frac{m_c(\theta)}{\rho_0 V_c(\theta)}\right)^n, \quad (3a)$$

$$T_c(\theta) = \left(T_0\frac{p_c(\theta)}{p_0}\right)^{\frac{n-1}{n}}. \quad (3b)$$

Here n is the polytropic index, m_c is the total cylinder mass, and ρ_0, T_0, and p_0 are the chamber density, temperature, and pressure at the beginning of the cycle. While the ideal gas model applies to both the intake and discharge process, the lack of a suction valve or other significant flow restriction in a rolling piston compressor

means that an assumption of quasi-static filling for the suction chamber can be justified. The chamber refrigerant state is thus fixed by the line conditions and port location.

3.3 Valve Dynamics

The dynamic behavior of the discharge valve has a major influence on flow pulsation levels. The design of a typical compressor reed valve is shown in Fig. 2. To include inertia, energy dissipation, and stiffness effects, the valve is modeled as a linear, single degree of freedom mass-spring-damper system (Fig. 3). Also included in the model are the valve preload, F_0, and the valve stop height, y_{vs}. The differential equation of motion for the system then becomes

$$\frac{d^2y_v(t)}{dt^2} + 2\zeta_v\omega_n\frac{dy_v(t)}{dt} + \omega_n^2 y_v(t) = \frac{F_p(t) - F_0}{m_v}, \tag{4a}$$

$$F_p(t) = [p_c(t) - p_d(t)]A_v(t), \tag{4b}$$

$$\omega_n = \sqrt{\frac{k_v}{m_v}}, \tag{4c}$$

$$\zeta_v = \frac{c_v}{2m_v\omega_n}. \tag{4d}$$

y_v	=	valve displacement
ζ_v	=	valve damping ratio
ω_n	=	undamped natural frequency
F_p	=	net valve pressure force
m_v	=	effective valve mass
p_c	=	compression chamber pressure
p_d	=	manifold pressure at valve
A_v	=	valve force area
k_v	=	effective valve stiffness
c_v	=	effective viscous damping coefficient

Displacement values from Eq. 4a are compared with the stop height after each program iteration. If the calculated displacement exceeds this limit, y_v is set equal to y_{vs}. The valve pressure force is determined from the pressure differential and force area, A_v. Valve force area can be assumed to be equivalent to the port area, computed analytically or determined experimentally. The effective mass, stiffness, and viscous damping coefficient are based upon experimental measurements of the valve's free vibration characteristics. Although actual compressor reed valves are multiple degree of freedom systems with a large number of natural frequencies, this simplified model is sufficient because the largest cylinder pressure harmonics do not strongly excite higher modes of vibration, nor do these higher modes significantly affect refrigerant flow rates.

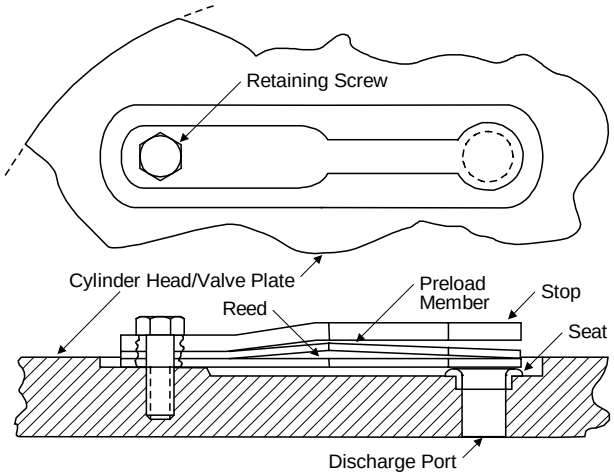

Figure 2 : Design details for a representative discharge valve

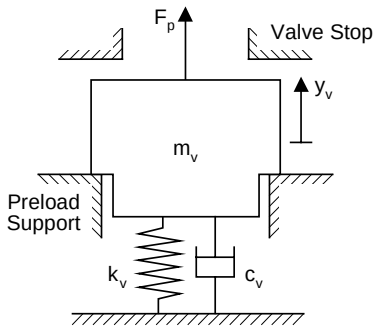

Figure 3 : Mechanical components of a rolling piston vapor compressor

3.4 Valve Flow Model

Discharge flow areas at discrete valve displacement values are entered into the program from an input data file. These values should be determined by the user, preferably by experiment. The discharge process is then modeled as steady, compressible, ideal gas flow through an orifice (Singh and Soedel, 1979):

$$m_v = C_d(\theta)A_f(\theta)p_u(\theta)\sqrt{\frac{2g_c}{(k-1)R_gT_u}\left[r_p(\theta)^{\frac{2}{k}} - r_p(\theta)^{\frac{k+1}{k}}\right]}, \quad (5a)$$

$$r_p = \frac{p_v}{p_u} \qquad (r_p > r_c), \quad (5b)$$

$$r_p = r_c \qquad (r_p \le r_c), \quad (5c)$$

$$r_c = \left(\frac{2}{k+1}\right)^{\frac{k}{k-1}}. \quad (5d)$$

m_v	=	discharge mass flow rate
C_d	=	valve discharge coefficient
A_f	=	effective valve flow area
p_u	=	upstream pressure
p_v	=	downstream pressure
g_c	=	gravitational constant
k	=	specific heat ratio
R_g	=	gas constant
T_u	=	upstream fluid temperature
r_c	=	pressure ratio for choked flow
r_p	=	pressure ratio

No significant restrictions exist in the suction line; thus, neglecting the inertia of the gas in the suction passages allows the nominal mass flow rate through the suction port to be determined kinematically using Eq. 2a and the fluid equation of state.

3.5 Acoustic Manifold Modeling

The compressor manifolds are modeled by discretizing the systems into subsystems whose dynamic behavior can be analytically described with four pole transfer matrices. In this scheme, linear acoustic elements are described in terms of input and output variables representing acoustic volumetric flow rate and acoustic pressure. An assumption of one-dimensional plane wave propagation limits the upper analysis frequency to

$$f_{\max} = \frac{c}{2D_{\max}}(\mathrm{Hz}), \quad (6a)$$

$$c = \sqrt{kR_gT}, \quad (6b)$$

where D_{max} is the hydraulic diameter and c is the sonic velocity in the gas medium.

Element boundaries usually represent discontinuities in the manifold system. These discontinuities are assumed to be abrupt to eliminate diffraction (Singh and Soedel, 1979; Rschevkin, 1963). The acoustic model consists of elements connected in series and parallel. A passage that has multiple section changes requires the use of several elements of appropriate size and type.

Six element types are utilized: (i) constant cross section tube, (ii) lumped volume cavity, (iii) identity connection, (iv) anechoic termination, (v) open termination, and (vi) closed termination. The most commonly used element is the constant cross section tube. Passages of this type are common in compressor manifolds, and their acoustic behavior is well understood. Both inertia and compliance effects are present in the analytical model, and energy dissipation can be taken into account through the use of an empirical damping factor (Singh and Soedel, 1979; Kammin, 1988).

Large cavities that appear in the system can be represented as lumped volumes. Unlike the constant cross section tubes, these elements model only fluid compliance effects. The identity connection allows specification of an output position, but does not affect the system dynamics or simulation results. The anechoic termination element represents an infinitely long duct in which acoustic waves propagate without reflection. An open tube with zero acoustic pressure at its boundary is modeled with an open termination element, while a closed termination simulates a rigid boundary with infinite impedance and zero volume velocity. The theory supporting the application of these models is well developed (Singh and Soedel, 1978, 1979; Kim and Soedel, 1988).

Coupling of the linear acoustic elements occurs in the frequency domain, and is based on two-port network theory. In the acoustic variant of this approach, we express the relationship between input and output variables for the i-th element in a manifold system as

$$p_{\mathrm{in}}(\omega) = A(\omega)p_{\mathrm{out}}(\omega) + B(\omega)q_{\mathrm{out}}(\omega), \quad (7a)$$

$$q_{\mathrm{in}}(\omega) = C(\omega)p_{\mathrm{out}}(\omega) + D(\omega)q_{\mathrm{out}}(\omega), \quad (7b)$$

$$\begin{Bmatrix} p(\omega) \\ q(\omega) \end{Bmatrix}_{\mathrm{in}} = [\Delta]_i \begin{Bmatrix} p(\omega) \\ q(\omega) \end{Bmatrix}_{\mathrm{out}}, \quad (8a)$$

$$[\Delta]_i = \begin{bmatrix} A(\omega) & B(\omega) \\ c(\omega) & D(\omega) \end{bmatrix}. \quad (8b)$$

Here the acoustic pressure, p, serves as the across variable, and the acoustic volume velocity, q serves as the

through variable. The transmission matrix, [Δ], is sometimes referred to as a four pole matrix. Four pole parameters A, B, C, and D depend on the element geometry and oscillation frequency, and like the acoustic variables, are generally complex valued.

Coupling techniques for series and branch connected transfer matrices are documented in the open literature, and so those equations are not included here. The result of the coupling operation is a complex valued, frequency domain description of the dynamic relationship between acoustic input and output variables. Equations 7a and 7b can be solved simultaneously for the acoustic pressures in terms of the volume velocities:

$$\left\{ \begin{array}{c} p_{\text{in}}(\omega) \\ p_{\text{out}}(\omega) \end{array} \right\} = \left[\begin{array}{cc} z_{11} & z_{12} \\ z_{21} & z_{22} \end{array} \right] \left\{ \begin{array}{c} q_{\text{in}}(\omega) \\ q_{\text{out}}(\omega) \end{array} \right\}, \tag{9}$$

$$z_I = z_{11} = \frac{p_{\text{in}}}{q_{\text{in}}}(\omega) = \frac{A(\omega)}{C(\omega)} \text{ (input impedance)}, \tag{10}$$

$$z_T = z_{12} = \frac{p_{\text{in}}}{q_{\text{out}}}(\omega) = \frac{1}{C(\omega)} \text{ (transfer impedance)}. \tag{11}$$

Note that the output impedance, z_{22}, is rarely of interest. A transfer function that does find use in a simulation program of this type is the acoustic pressure ratio:

$$\frac{p_{\text{out}}}{p_{\text{in}}}(\omega) = \left(\frac{p_{\text{out}}}{q_{\text{in}}} \right) \left(\frac{q_{\text{in}}}{p_{\text{in}}} \right) = \frac{z_{21}}{z_{11}} = \frac{1}{A(\omega)}. \tag{12}$$

The transfer functions of Eqs. 10-11 represent a complete frequency domain description of the manifold.

3.6 Coupling Compressor and Manifold Models

The simulation program must model the acoustic effects of pressure pulsations on the physical processes that occur in the compressor body during compression and expansion of the refrigerant. However, simulation iterations and cylinder processes calculations occur in the time domain, while acoustic effects are introduced through frequency domain calculations. The discrete Fourier transform (DFT) and acoustic impedance definitions of Eqs. 10 and 11 are used to couple the two. Consider a process yielding an initial mass flow rate profile consisting of i = 1, 2, ..., M equally spaced discrete values. We begin by applying a DFT and expressing the profile as a finite Fourier expansion written in terms of the crank angle:

$$\dot{m}(\theta_i) = \frac{M_0}{2} + \sum_{n=1}^{N} M_n \cos(n\theta_i - \psi_n), \tag{13}$$

$$M_n = \sqrt{a_n^2 + b_n^2} \tag{14a}$$

$$\tan(-\psi_n) = \frac{b_n}{a_n}, \tag{14b}$$

$$a_n(n\omega_0) = \frac{1}{M} \sum_{i=0}^{M-1} \dot{m}_v(\theta_i) \cos(n\theta_i), \tag{15a}$$

$$b_n(n\omega_0) = \frac{1}{M} \sum_{i=0}^{M-1} \dot{m}_v(\theta_i) \sin(n\theta_i), \tag{15b}$$

M_n	=	mass flow harmonic magnitude
ψ_n	=	mass flow harmonic phase
N	=	number of crank harmonics in the expansion
n	=	crank speed harmonic index
a_n	=	discrete Fourier cosine coefficient
b_n	=	discrete Fourier sine coefficient
M	=	number of crank points in a simulation cycle

Equation 13 serves as the time domain representation of the function while Eqs. 14a and 14b are the frequency domain representation. Volume velocities are obtained by dividing Eq. 13 by the average suction or discharge line refrigerant density. The corresponding fluid states are used to calculate the sonic velocity in the valve chamber and suction line. These values are in turn used to develop the four pole matrices containing the input and transfer impedance values. The product of the volume velocity and transfer or input impedance then yields the frequency domain acoustic manifold pressures at the discharge valve (p_1) and a second, user specified manifold location (p_2):

$$p_1(n\omega) = z_I(n\omega) q_1(\omega), \tag{16a}$$

$$p_2(n\omega) = z_T(n\omega) q_1(\omega). \tag{16b}$$

An inverse discrete Fourier transform (IDFT) reconstructs the acoustic pressures in the time domain, and the new profiles are used to correct mass flow rates during the next iteration.

4 Simulation Program Structure

Figure 4 shows a flowchart of the RSIMP program structure. The simulation is initiated by an input data file con-

taining compressor geometric information, fluid properties, valve characteristics, and element parameters for the manifold systems. A control variable indicates whether the discharge valve force area is assumed equal to the port area, or entered as a table of data with the area tabulated at discrete valve displacements. The discharge flow area is controlled and specified in a similar fashion. Valve parameters are entered in the form of the static stiffness, fundamental frequency, equivalent viscous damping ratio, preload force, and valve stop height.

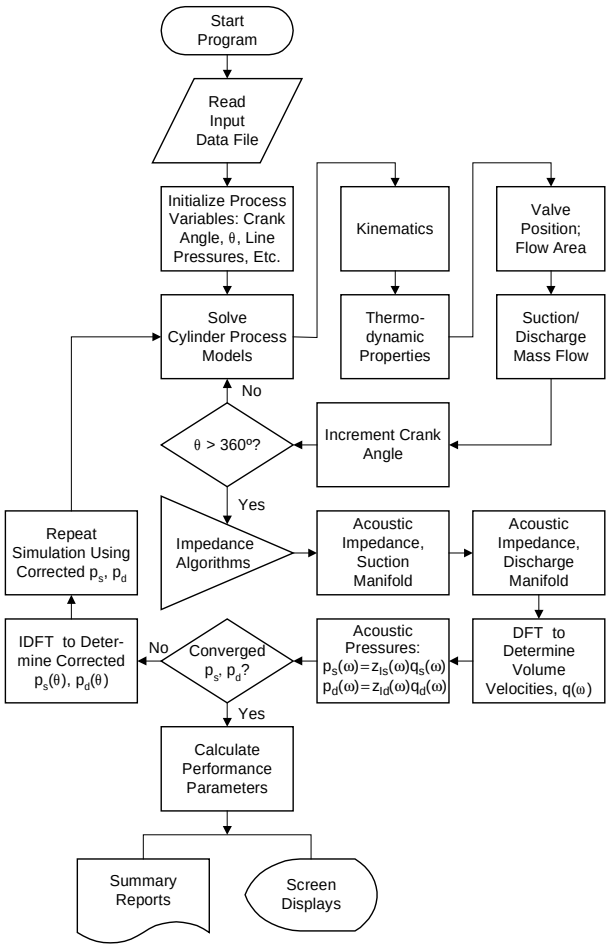

Figure 4 : Program structure

Several preliminary calculations are made to initialize the main simulation loop. These include determining the pressure ratio for choked flow, initial refrigerant density, pressure and impedance reference values, and effective mass of the discharge valve. The main iteration loop simulates one crank rotation cycle. In the physical machine, compression and charging occur simultaneously, and RSIMP models the processes simultaneously. At each crank step, a mass balance and equation of state are applied to each control volume. Upon completion of a crank rotation, the final suction state becomes the initial discharge state for subsequent iterations.

The most important part of the simulation is the interaction between the chamber pressures and manifold pressures. These processes are rather straightforward on the discharge side. The valve equation of motion, compression chamber equation of state, and fluid flow equation are all solved simultaneously using a fourth-order Runge-Kutta technique. For the first iteration, the discharge pressure is assumed constant and the initial mass is specified by the maximum discharge chamber volume and mean suction pressure. A discrete Fourier transform is applied to the computed mass flow rate, and these values are used with the discharge acoustic input impedance to compute a corrected line pressure profile. The new pressures then provide more exact mass flow values during the next iteration, which in turn lead to an even more accurate pressure profile. At the start of each discharge iteration beyond the initial loop, mass balance and pressure results from the suction simulation provide more exact initial refrigerant states.

The suction simulation is quite different. The lack of a port valve means that pulsations in the suction line have a direct and immediate effect on the mass flow rate. Because the inertia of the gas is neglected, the suction volume velocity (volumetric flow rate) is fixed by the crank speed and kinematic differential volume relation. This value is used with the suction manifold input impedance to determine an initial approximation for the suction line acoustic pressures, which are then used with the equation of state to compute a corrected mass flow profile. The main iteration loop is repeated until average mass flow rates and manifold pressure profiles converge to within a specified criterion.

Post-processing routines conclude the simulation by calculating cyclic performance parameters such as volumetric efficiency, performance index, work per cycle, power and torque required, mean and extreme pressure values, and net mass flow per cycle. For example, the total piston work per cycle is given as:

$$W_{\text{cycle}} = -\int_{\text{cycle}} pdV. \tag{17}$$

Suction underwork and discharge overwork are calcu-

lated in a similar fashion, with the pressure term in Eq. 17 being replaced by the difference between the chamber pressure and average acoustic pressure at the port. The program also calculates:

- Power required
- Torque required
- Performance index
- Average mass flow rate
- Average temperature in the working volume, discharge manifold, and suction manifold
- Maximum, minimum, and average pressures in the working volume, at the discharge valve, in the discharge line, and in the suction line

5 Program Output

Results are presented in both tabular and graphical form. Tabular output echoes the input data, lists calculated performance parameters, and displays volume, temperature, chamber and line pressure, instantaneous mass flow rate, and valve displacement as a function of the crank angle. Frequency domain results consist of impedance transfer function values, as well as pressure and mass flow rate harmonic data. The graphical displays include seven plots:

Suction/Discharge Chamber Pressure Versus Crank Angle The cylinder pressure profile is plotted from $\theta = 0^\circ$, where the compression volume is maximized, to 360°, where the compression volume approaches zero.

Suction and Discharge Line Pressure Versus Crank Angle These curves explicitly show the pressure pulsations present in the manifolds at the suction and discharge ports. The suction volume pressure is identical to the suction line pressure. These curves can be displayed either separately or with the compression volume pressure. An experienced analyst is able to interpret the phasing of the line and chamber pressures and determine whether the interaction helps or hinders the flow processes.

Discharge Valve Displacement Versus Crank Angle This plot is displayed simultaneously with the chamber and line pressures, and is useful in the design of the valve reed and stop.

Instantaneous Mass Flow Rates Versus Crank Angle These plots allow any back flow through the suction or discharge ports to be identified, and also play a major role in the acoustic tuning process by indicating suction flow profiles that help maximize capacity.

Chamber Pressure Versus Chamber Volume A standard pV diagram depicts the thermodynamic cycle over two crank rotations. From a control mass standpoint, charging and compression occur over 720°, compression and two rotations are shown to allow depiction of the complete depict the entire cycle.

Manifold Impedance Transfer Functions These values are computed and displayed as a function of either crank speed harmonic index (these are the transfer function values actually used in the simulation), or frequency for a user-specified range (useful for identifying acoustic resonance frequencies). Large magnitude, low frequency impedance harmonics have a significant effect on mass flow rates, while or a large magnitude, low frequency harmonics can create objectionable noise.

Pressure and Flow Rate Spectra This frequency domain information complements the time domain displays of these profiles. Used with the manifold system transfer functions, it helps a designer tune the manifold geometry so that only desirable resonance peaks are excited.

6 Example Application

To illustrate its use, RSIMP was applied to a household refrigerator compressor with the input parameters shown in Table 1. The manifold systems in vapor compressors tend to be rather complex, and to facilitate display of their acoustic models, we developed a graphical representation scheme for use with RSIMP. This scheme uses element depictions that are scaled according to hydraulic diameter and effective length (constant cross-section elements) or spherical diameter (lumped volume elements). Branches, terminations, and response output positions are depicted. An unscaled version of the schematic can also be displayed.

Figure 5 shows scaled and unscaled schematics for the example application's discharge and suction manifolds. The discharge manifold model consists of 14 elements comprising the main branch and three side branches (Fig 5a). Element 1 (lumped volume) is an irregular cavity in the volume cup (a muffling element not shown in Fig. 1) located directly above the discharge valve. Element 2

Table 1 : Example application input parameters

Parameter	Value
Cylinder radius (cm)	2.169
Roller radius (cm)	1.921
Cylinder height (cm)	1.651
Eccentricity (cm)	0.2471
Vane thickness (cm)	0.4064
Crank speed (rev/sec)	60.0
Nominal suction pressure (MPa)	0.1551
Nominal discharge pressure (MPa)	1.3445
Valve fundamental frequency (Hz)	155
Valve stiffness (N/m)	0.02984
Valve damping ratio	0.1
Valve preload force (N)	0.112
Valve stop distance (cm)	0.0381
Suction port area (cm^2)	0.3555
Discharge port area (cm^2)	0.1123

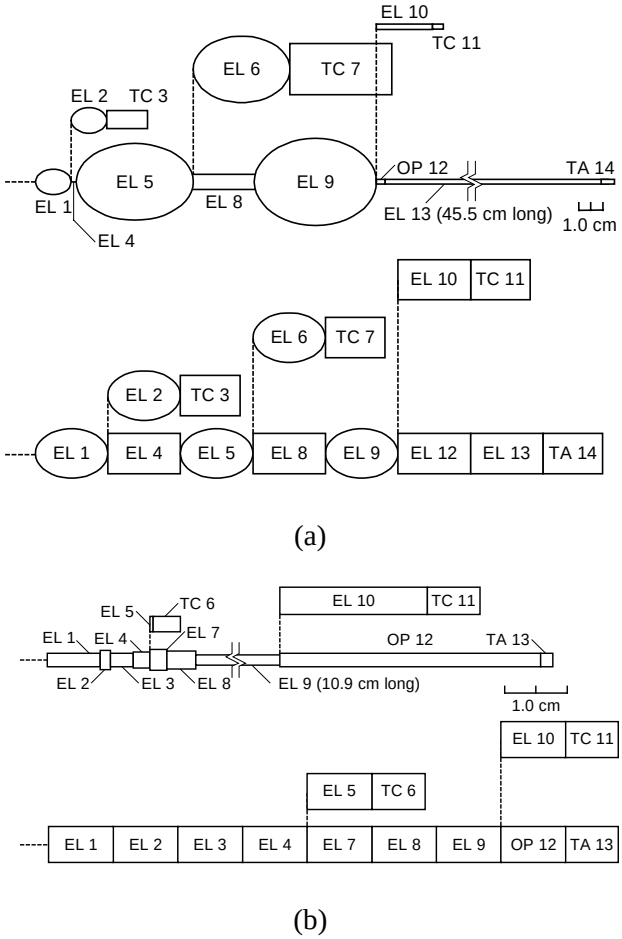

Figure 5 : Scaled and unscaled acoustic schematics for the (a) discharge manifold and (b) suction manifold

(lumped volume) is a volume cup cavity opposite the discharge valve. Because it does not lie along the primary refrigerant flow path, this volume is modeled as a side branch, and terminated by element 3, a closed termination.

Element 4 (constant cross section tube) is so small that it is barely discernible on the scaled schematic. Physically, it represents a clearance between a flange on the volume cup and a shaft journal bearing. The refrigerant flows through this tiny passage, which acts to isolate the subsystem preceding element 4 from elements 5-14. Consequently, small changes to the flange geometry produce significant changes in the location of impedance resonances and anti-resonances. Major modifications to elements 5-14 produce little change in the acoustic behavior.

Element 5 (lumped volume) is a cavity between the volume cup and motor rotor. This cavity is part of the main refrigerant flow path. Element 6 (lumped volume) is the oil sump cavity below the compressor cylinder. Like element 2, this volume is not part of the primary refrigerant flow path, so it is modeled as a side branch. It is terminated by element 7, a closed termination. Element 8 (constant cross section tube) is an annular passage between the motor rotor and stator. Element 9 (lumped volume) is a large cavity between the top of the rotor and the top of the shell.

Element 10 (constant cross section tube) is a crimped charging tube at the top of the shell. This side branch is terminated by element 11, a closed termination. Element 12 (constant cross section tube) is a short fitting used to mount a piezoelectric pressure transducer to the discharge line just outside the shell. This fitting was machined to have the same diameter as the discharge line. Because it was a measurement point in an experimental test stand used for RSIMP validation, it was chosen as the output element in the analytical model. Element 13 (constant cross section tube) is the discharge line between the transducer fitting and the condenser. This very long tube is terminated with an anechoic termination, element 14, since the vapor phase of the refrigerant extends for a considerable distance into the heat exchanger, preventing the reflection of propagating acoustic waves.

The suction manifold model (Fig. 5b) consists of 13 ele-

ments and two side branches. Element 1 (constant cross section tube) models the suction port, which consists of a cylindrical passage bored into the cylinder wall. Element 2 (constant cross section tube) is an oversized bore at end of the suction port that accommodates a fitting between the shell and port. Element 3 (constant cross section tube) is a cylindrical fitting between fitting between the shell and port. Element 4 (constant cross section tube) is a short cylindrical tube passing through the shell. Element 5 (constant cross section tube) is a very short reentrant section in the shell seal resulting from manufacturing tolerances. This small element has almost no effect on the system frequency response characteristics, and its branch is terminated by element 6, a closed termination. The exterior portion of the suction line shell seal

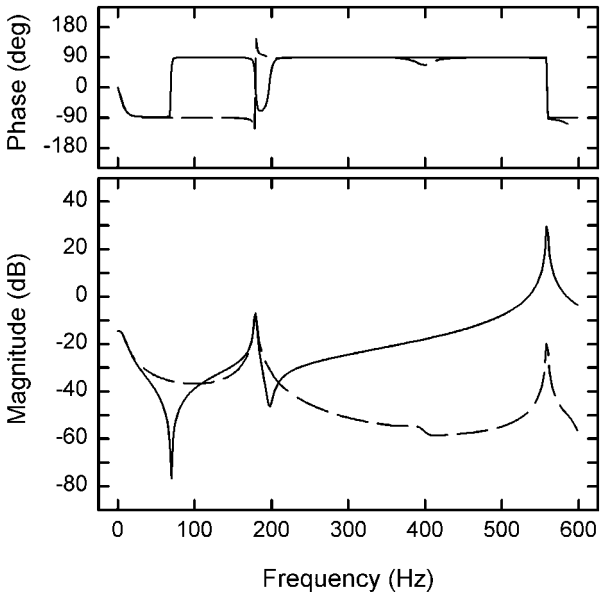

Figure 6 : Discharge manifold impedance transfer functions, input impedence (–); transfer impedance (– –)

is modeled by element 7 (constant cross section tube). Element 8 (constant cross section tube) models the oversized end of the suction line where it is soldered into the shell seal. Element 9 (constant cross section tube) is the suction line between the shell and accumulator. Element 10 (constant cross section tube) is the reentrant section of an accumulator used to trap liquid refrigerant. Its branch is terminated by element 11, a closed termination. Element 12 (constant cross section tube) models the suction line coming from the evaporator. It is terminated with an anechoic termination, element 14.

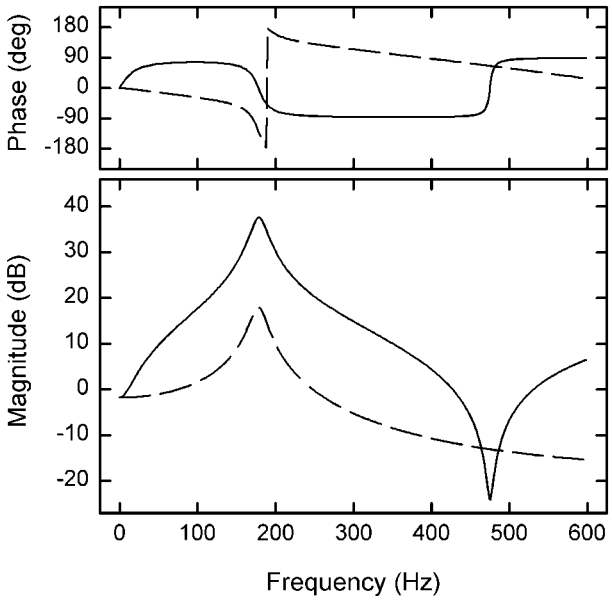

Figure 7 : Suction manifold impedence transfer functions, input impedence (–); transfer impedance(– –)

The acoustic impedance transfer functions for the two manifolds are shown in Figs. 6 and 7. Note the resonances that lie within the 0-600 Hz range of the plots. The lowest of these is near 180 Hz., a value corresponding to the third harmonic of the crank angular velocity. Proximity of a resonance peak to a low motor harmonic usually simplifies the tuning process.

Figure 8 shows cylinder process results from the simulation. Note in particular the prominent discharge line pulsations. With an amplitude of approximately 0.03 MPa, these pressure fluctuations have a significant effect on the discharge process. Suction line pulsations, on the other hand, are so low (0.006 MPa) that they are not apparent on the pressure scale used in the figure. The discrepancy is due in large part to the compressor's lack of a suction valve. Figure 9 shows that the suction mass flow rate profile has a longer duration and smaller maximum value than the discharge profile. These differences translate into lower suction volume velocity magnitudes at the crank speed harmonics, and less excitation of the suction manifold's acoustic modes.

Next, consider the discharge valve displacement profile in Fig. 8. The valve begins to open at a crank angle of 262°. There then exists an interval of nearly 10° during which the valve is opening and the compres-

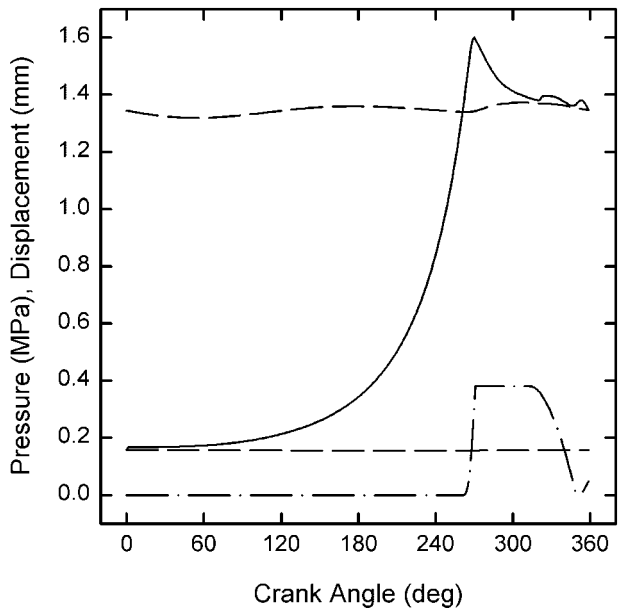

Figure 8 : Representative program results, compression chamber pressure (—-), discharge and suction line pressures (– –), and discharge valve displacement($\cdot - \cdot -$) versus crank angle.

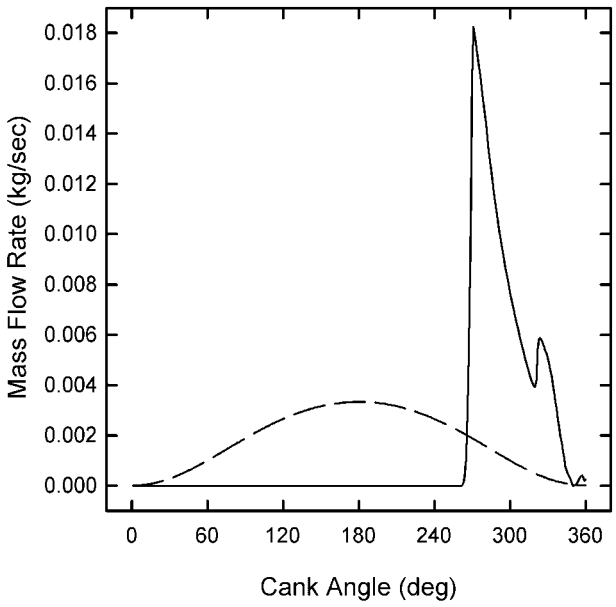

Figure 9 : Discharge mass flow rate (—-) and suction mass flow rate (– –) versus crank angle

sion chamber pressure increases to its maximum value. An ideal zeroth order valve would open instantaneously and minimize the compressor's energy consumption during the discharge process. Valves with low fundamental frequencies respond more slowly, resulting in higher flow impedance during this interval, and increased energy consumption. The valve contacts the stop at θ = 271°, the chamber pressure drops slightly, and the discharge process proceeds with the valve fully open.

Valve dynamics again begin to affect the cylinder processes near θ = 314°, when the valve starts to close. The cylinder pressure oscillations and discharge mass flow rate fluctuations (Fig. 9) seen in this part of the cycle can excite line pressure pulsations that in turn affect the discharge overwork, energy consumption, and noise levels. Note that the valve closes before the cycle is completed, but then reopens slightly, a phenomenon that has been noted by other investigators. Overall, the predicted valve behavior is consistent with the physical constraints on the system.

The simulation for this example case converged after 7 crank cycle iterations. After some large, 8-12 percent changes during the early iterations while the line pressure profiles are being established, the final average discharge mass flow rate (one of the variables used as a convergence criterion) is quickly achieved. Validation testing shows that convergence usually occurs within 20 iterations.

7 Experimental Validation

Chamber pressure and refrigerant flow rate predictions from the simulation program were compared with existing experimentally measured pressure and performance data provided by the project sponsor. Agreement was quite good. In addition, manifold acoustic pressure predictions were confirmed through a set of tests on a rolling piston compressor mounted in a refrigerator test stand. Piezoelectric pressure transducers were installed in the shell and at various points in the suction and discharge lines. Both time and frequency domain pressure data was collected.

Data from each of the measurement points matched the simulation results closely. For example, Fig. 10a shows time domain acoustic pressures measured in the discharge line just outside the shell. Figure 10b shows RSIMP predictions at the same point. The pulsation level at this location in the line is quite small, about 0.003 MPa peak-to-peak. The simulation and experimental profiles

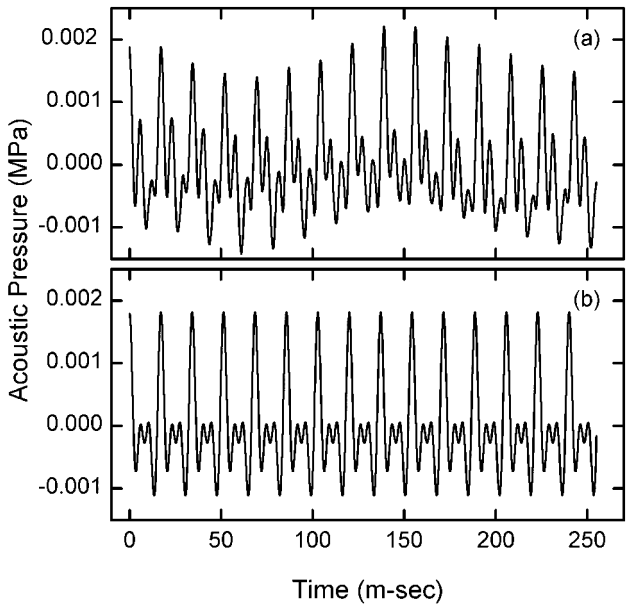

Figure 10 : Comparison of experimental and analytical pulsation results, (a) time domain discharge line pressure measured near shell exit, (b) corresponding profile from simulation program.

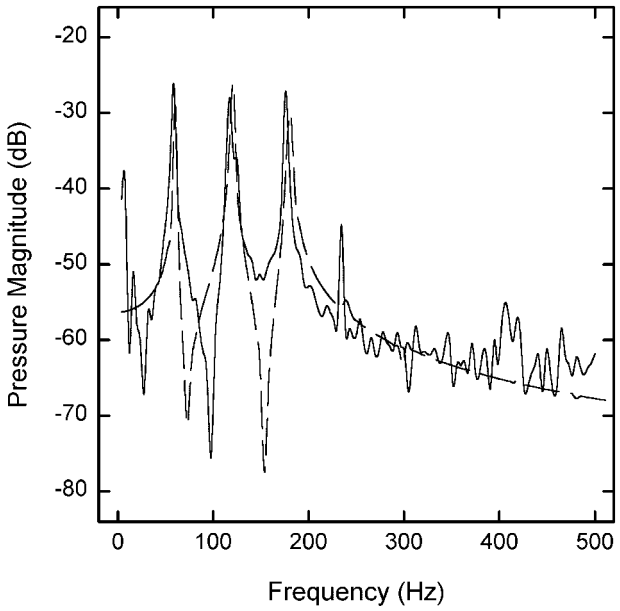

Figure 11 : Frequency spectrum amplitudes for experimentally measured (—-) and computer predicted (– –) discharge manifold pressure pulsations.

are similar in amplitude and form. The small amplitudes are due to the measurement location, which was well downstream from muffling elements near the discharge valve. As noted earlier, the program predicts much larger pressure amplitudes near the discharge valve. Agreement between the computed and experimentally measured discharge manifold pressure frequency spectrum amplitude was also quite good (Fig. 11).

8 Conclusions

RSIMP has proven to be a practical, effective tool for simulating the mechanical, thermodynamic, fluid, and acoustic processes in a stationary-vane, rolling piston compressor. As presented here, our work makes three contributions: the solution algorithm itself, the techniques used for displaying and interpreting acoustic manifold schematics, and the validated example case results, which are representative of the behavior of this type of fractional horsepower refrigeration compressor.

Early versions of RSIMP used Fortran 90 as the development environment. However, the latest version was ported to Microsoft Visual Basic so that a Windows graphical user interface could be added to the manifold modeling routines. While this language does not offer the portability of other programming languages - C/C++, for example - the ubiquitous nature of the Windows operating system makes Visual Basic a good choice for an application-oriented program such as RSIMP.

The simulation program could be improved by developing more accurate models for the compressor components and processes that most influence steady state operation. These enhancements might include variable crank speed, a multiple degree of freedom valve model, fluid leakage (particularly at the piston-cylinder interface), and nonlinear effects due to mean fluid flow.

A deterministic modeling approach is now used throughout the algorithm. It might be possible to use stochastic representations for critical processes and component parameters; however, such data are rarely found in the open literature, particularly for rolling piston compressors, and generation of the data was beyond the scope of this project. Another enhancement would use empirical data along with inverse techniques to optimize model parameters. The manifold modeling process can be improved by defining new acoustic elements that integrate experimental impedance measurements or acoustic finite element results into the simulation. Finally, in an effort

to model the effect of tuning resonators, RSIMP has been modified to include a third acoustic manifold system coupled only to the cylinder processes, and independent of the suction and discharge processes.

9 Acknowledgments

General Electric Appliances supported this work under a contract administered through the University of Louisville Research Foundation.

10 References

Chai, G.B.; Ooi, K.T. (1995): Analysis of vane-spring structures. *Computers & Structures*, vol. 57, no. 3, pp. 447-453.

Hadfielda, M.; Safarib, S. (1998): Wear behaviour of the piston/gudgeon pin in a hermetic compressor with replacement CFC refrigerants. *Wear*, vol. 219, no. 1, pp. 8-15.

Hamilton, J.F. (1974): Extensions of mathematical modeling of positive displacement type compressors. Research report, Purdue University.

Ishii, N.; Imaichi, K.; Muramatsu, S. (1984): The study of rolling piston, rotary compressor dynamic behavior when stopping to reduce noise and vibration level. In: *Proceedings of the international compressor engineering conference at Purdue*.

Itami, T.; Kubo, M.; Sugiyama, M. (1986): Estimation of bearing load of rolling piston type rotary compressors under high speed operation. In: *Proceedings of the international compressor engineering conference at Purdue*.

Jorgensen, S.H.; Nissen, H.S. (1984): Mechanical loss model of rolling piston rotary compressor with special importance attached to journal bearing. In: *Proceedings of the international compressor engineering conference at Purdue*.

Kammin, H. (1988): The development and experimental verification of an acoustic damping model for a frequency domain digital pulsation simulation. In: *Proceedings of the international compressor engineering conference at Purdue*.

Kim, J.; Soedel, W. (1988): Four pole parameters of shell cavity and application to gas pulsation modeling. In: *Proceedings of the international compressor engineering conference at Purdue*.

Lin, H.; Atluri, S.N. (2000): Meshless local Petrov-Galerkin (MLPG) method for convection-diffusion problems. In: *Computer Modeling in Engineering and Sciences*, vol. 1, no. 2, pp. 45-60.

Lin, H.; Atluri, S.N. (2001): The meshless local Petrov-Galerkin (MLPG) method for solving incompressible Navier-Strokes equations. In: *Computer Modeling in Engineering and Sciences*, vol. 2, no. 2, pp. 117-142.

Nieter, J. (1983): Computer simulation and modal analysis study of compressor manifolds and tuning phenomena. M.Sc. thesis, Ohio State University.

Okada, K.; Kuyama, K. (1982): Motion of rolling piston in rotary compressor. In: *Proceedings of the Purdue compressor technology conference*.

Okoma, K.; Onoda, I. (1988): Study of lubrication mechanism for horizontal type rolling piston rotary compressor. In: *Proceedings of the international compressor engineering conference at Purdue.*

Ooi, K.T.; Wonga, T.N. (1997): A computer simulation of a rotary compressor for household refrigerators. In: *Applied Thermal Engineering*, vol. 17, no. 1, pp. 65-78.

Ooi, K.T.; Chai, G.B.; Kwek, E.C. (1992): A simple valve model to study the performance of a small compressor. In: *Proceedings of the 1992 international compressor engineering conference at Purdue*, pp. 147-155.

Padhy, S.K.; Dwivedi, S.N. (1994): Heat transfer analysis of a rolling-piston rotary compressor. In: *International Journal of Refrigeration*, vol. 17, no. 6, pp. 400-410.

Park, Y.C.; Kim, Y.C.; Min, M.K. (2001): Performance analysis on a multi-type inverter air conditioner. *Energy Conversion and Management*, vol. 42, no. 13, pp. 1607-1621.

Rschevkin, S.N. (1963): A course of lectures on the theory of sound. McMillian Co., New York.

Rugonyi, S.; Bathe, K.J. (2001): On Finite Element Analysis of Fluid Flows Fully Coupled with Structural Interactions, *CMES:Computer Modeling in Engineering & Sciences*, vol. 2, no. 2, pp. 195-212.

Sa, B.D.; Kim, K.H.; Son, S.H.; Park, Y.D.; Byun, C.H. (1992): The design optimization and experimental behavior of the valve for a rolling piston type rotary compressor. In: *Proceedings of the 1992 international compressor engineering conference at Purdue*, pp. 127-136.

Sartre, V.; Lallemand, M.; Chiaffi, M. (1994): Tech-

nological advances of compressors in refrigerating machines. *International Journal of Refrigeration*, vol. 17, no. 3, pp. 156-165.

Sheiretov, T.; Van Glabbeek, W.; Cusano, C. (1995): Simulaive friction and wear study of retrofitted swash plate and rolling piston compressors. *International Journal of Refrigeration*, vol. 18, no. 5, pp. 330-335.

Singh, R.; Soedel, W. (1979): Mathematical modeling of multicylinder compressor discharge system interactions, *J Sound Vibration*, vol. 63, pp. 125-143.

Singh, R.; Soedel, W. (1978): Assessment of fluid-induced damping in refrigeration machinery manifolds, *J Sound Vibration*, vol. 57, pp. 449-452.

Soedel, W. (1972): Introduction to computer simulation of positive displacement type compressors. Research report, Purdue University.

Yanagisawa, T.; Shimizu, T.; Horioka, T. (1988): A study on starting characteristics of a rolling piston type rotary compressor. In: *Proceedings of the international compressor engineering conference at Purdue*.

Yanagisawa, T.; Shimizu, T. (1982): Motion analysis of rolling piston in rotary compressor. In: *Proceedings of the Purdue compressor technology conference*.